Dev. Chem. Eng. Mineral Process., 11(5/6), pp. 603-620, 2003.

Crystallization of Boric Acid through Reactive Dissolution of Oxalic Acid Crystals in Aqueous Borax Solution

B. ZareNezhad[*] and J. Garside[#]

Ministry of Science, Research and Technology, PO Box 15875-4786, Tehran, Iran

[#]Dept of Chemical Engineering, UMIST, PO Box 88, Manchester M60 1QD, England

In the reaction between solid oxalic acid and aqueous borax solution, product boric acid precipitates in the solution phase after complete dissolution of oxalic acid crystals. This makes it possible to measure the dissolution and precipitation kinetics independently. The oxalic acid dissolution process was found to be diffusion controlled. Nucleation rates of product boric acid were influenced by heterogeneous primary nucleation and secondary nucleation, while growth rates were affected by both the bulk diffusion and surface integration processes. Dissolution of oxalic acid crystals was described by a surface reaction model, and overall nucleation and growth rates were correlated in terms of the influencing process variables. Simulation analysis was carried out by linking the two processes of dissolution and precipitation in series. The trends of the predicted supersaturation profiles, number concentration, magma density and mean size of the product crystals are in good agreement with measured values.

Introduction

Reactive crystallization processes are widely used for the production of many valuable chemicals. There are many different studies in this field which are mainly confined to liquid-liquid reactions (Franck et al., 1988; Tavare and Garside, 1990; David et al., 1996) and to some gas-liquid reactions (Wachi and Jones, 1991; Mullin, 1993). In the case of a solid-liquid reaction, if the solid reactants start dissolving and the fluid phase becomes supersaturated with respect the reaction product, then precipitation from the fluid phase may occur (ZareNezhad et al., 1996; ZareNezhad, 1996). Since it is usually difficult to distinguish between the product crystals and the reactant particles, the kinetics measurements cannot be performed.

* *Author for correspondence (zarenezhad@yahoo.com).*

In this work, the reactive crystallization of boric acid from borax solution and oxalic acid crystals was investigated in a batch mode. The overall reaction can be represented by:

$$Na_2B_4O_7 .10H_2O_{(aq)} + (COOH)_{2(S)} \rightarrow (COONa)_{2(aq)} + 4\ H_3BO_{3(S)} + 5\ H_2O \qquad (1)$$

For this system, the precipitation of product boric acid takes place after complete dissolution of the solid reactant. The kinetics of oxalic acid dissolution in borax solution are determined, and the subsequent nucleation and growth kinetics of boric acid crystallization are characterized. The process simulation analysis is used to explore the effects of different process variables.

Experimental Procedure

The crystallizer used was a 1.5-litre jacketed baffled cylindrical vessel (11 cm i.d., height 16 cm) maintained at constant temperature. A six-blade stainless steel disk turbine impeller with a clearance of 2.5 cm from the bottom was used to ensure that all particles were completely suspended. The stirrer was rotated by a variable-speed stirrer motor (RZR-200, Heidolph), and the impeller speed set at the required values using a digital tachometer (Heidolph) attached to the motor. Both pH and temperature were recorded.

In a typical experiment the required amount of water was first filtered and then charged into the crystallizer. Borax and boric acid crystals were added and the contents were stirred to dissolve the crystals and a clear solution of known composition was obtained. A known amount of oxalic acid crystals, sieved in the size range of 320-1200 μm, was quickly added to the solution at the start of an experiment. The addition point was carefully fixed (using a plastic funnel) throughout the series of experiments to be midway between the centre of the precipitator and the vessel wall. Sampling was achieved by pipetting 5 ml of the contents from the crystallizer at different time intervals and filtering it through 0.4 μm pore size filter paper. The pipette tip diameter was 3 mm, adequate for collecting the product crystals in the size range of 8-130 μm. In some experiments the sampling accuracy was checked by simultaneous pipetting two samples of the slurry from the same level of impeller from two symmetrical points at the opposite sides of the crystallizer. Since the crystal size distributions of these two typical samples were very similar, it was concluded that the sampling technique led to reproducible results and good homogeneous mixing was satisfied.

The samples of solids and filtrates were weighed and finally analysed to determine changes in the overall compositions of the solid and solution phases during the process. The fractional conversion of the solid reactant, where X = (mass of reacted oxalic acid crystals)/(mass of original oxalic acid crystals), versus time was measured. A dual pH titrimetric method was used to determine the composition of borax and boric acid in the solution phase (Jeffery et al., 1989). A measured quantity of the solution-phase sample was diluted with 50 ml of distilled and filtered water. The solution was first titrated with 0.05 M sulphuric acid for determination of borax concentration, and then back-titrated with 1.0 M sodium hydroxide solution using the correct amount of mannitol for evaluating the boric acid concentration. The sodium

analysis was carried out by atomic absorption spectrophotometry at a wavelength of 589 nm. Samples of the solid phase were also analysed for crystal size distribution using a multi-channel Coulter counter (Model Multisizer II) equipped with a 400 μm orifice tube. The solid samples collected on the filter paper were quickly dispersed into the Coulter cell containing filtered Isoton II saturated with boric acid and oxalic acid. In some experiments the analysis was performed twice for an identical sample so that any change of crystal size distribution could be detected. These sets of crystal size distribution of the same sample were very close to each other and therefore, in this case, all sets of crystal size distributions were averaged. A series of experiments was carried out at different operating conditions covering the ranges of the variables shown in Table 1.

Table 1. *Ranges of process variables for the reactive crystallization of boric acid.*

Run	c_{B0} ***(mol/kg)***	N_{so}/M ***(mol/kg)***	N ***(Hz)***	L_{A0} ***(μm)***	T ***(K)***
R1 - R6	0.04-0.14	0.04-0.14	7	320	293
R7 - R12	0.05	0.05	8-18	1024	293
R13- R18	0.07	0.07	11	320-1200	293
R19- R24	0.11	0.11	10	320	293-313

Modelling of the Process

(i) Dissolution kinetics of oxalic acid crystals

The experimental measurements indicated that the reaction of borax solution with oxalic acid crystals was fast and took place very near to the oxalic acid crystal surface. Therefore, the diffusion through the liquid film surrounding the solid surface is controlling the overall dissolution process. In order to obtain the relation between conversion and time, the rate of disappearance of solid oxalic acid (A), R_A, must be equated with the rate of consumption of borax (B). From the reaction stoichiometry:

$$R_A = -\frac{1}{A_{ex}}\frac{dN_s}{dt} = \frac{N_{so}}{A_{ex}}\frac{dX}{dt} = \rho_l \beta k_d c_B \qquad (2)$$

where N_s is the number of moles of solid reactant (oxalic acid); A_{ex} is the external surface of spherical oxalic acid crystals; ρ_l is the density of free water; β is the stoichiometric coefficient of the reactants (which is equal to 1 by Equation 1); c_B is the borax concentration in the solution phase; and k_d is the solid-liquid mass transfer coefficient.

For the range covered experimentally in the present study ($0.5 < Re_p < 600$ and $700 < Sc < 1200$), the correlation proposed by Asai et al. (1986) is used for determination of the solid-liquid mass transfer coefficient. This correlation can be written as:

$$Sh = 2 + 0.61\, Re_p^{0.58}\, Sc^{1/3} \tag{3}$$

where $Sh = k_d L_A / D_A$; $Re_p = L_A^{4/3} (N_p \rho_s N^3 D^5 / V)^{1/3} / \nu$; $N_p = 6$ (for disk turbine); and $Sc = \nu / D_A$.

Equation (3) for determination of solid-liquid mass transfer coefficient can be written as:

$$k_d = D_A [2L_A^{-1} + 0.61 (\frac{\rho N_p D^5}{V \nu^3})^{0.19} L_A^{-0.22} N^{0.58}] \tag{4}$$

From Equation (1), the variation of borax (B) concentration with solid oxalic acid conversion, X, can be written as:

$$c_B = c_{Bo} (1 - \frac{N_{so}}{Mc_{Bo}} X) \tag{5}$$

where M is the mass of free water.

During the dissolution process, the oxalic acid crystals shrink in size and thus: particle diameter at any time during the reaction can be obtained by the relation:

$$L_A = L_{Ao} (1 - X)^{1/3} \tag{6}$$

where L_{Ao} is the initial mean diameter of oxalic acid crystals; and L_A is the average diameter at solid reactant conversion, X.

Combining Equations (2), (5) and (6), the rate of solid oxalic acid conversion can be derived as:

$$\frac{dX}{dt} = 6 \frac{\rho_l k_d c_{Bo}}{\rho_s L_{Ao}} (1 - X)^{2/3} (1 - \frac{N_{so}}{Mc_{Bo}} X) \tag{7}$$

According to Equation (1), the variation of boric acid (BA), borax (B) and sodium oxalate (S.ox) concentrations with solid oxalic acid conversion can be written as:

$$\frac{dc_{BA}}{dt} = 4\frac{N_{so}}{M}\frac{dX}{dt} - \rho_s k_v \frac{dm_3}{dt} \tag{8}$$

$$\frac{dc_B}{dt} = -\frac{dS_{.ox}}{dt} = -\frac{N_{so}}{M}\frac{dX}{dt} \tag{9}$$

where $c_{BA} = c_{BAo}$; $c_B = c_{Bo}$; and $c_{S.ox} = X = m_3 = 0$ at $t = 0$. Equation (8) links the oxalic acid dissolution and boric acid crystallization processes through the third moment of CSD.

(ii) Precipitation kinetics of boric acid

Nucleation kinetics

The variations of the number of product crystals with stirrer speed shown in Figure 6 indicate the occurrence of both primary and secondary nucleation. Assuming that the total nucleation rates produced by the two mechanisms are additive (Mullin, 1993), then the overall nucleation rates, B, may be written as:

$$B = K_p \exp\left[-\frac{\alpha \varphi^2 \gamma^3}{(kT)^3 (\ln S)^2}\right] + K_s (S-1)^b M_T^j N^h \exp(-E_S/RT) \tag{10}$$

where the first and second terms in Equation (10) represent the primary nucleation rate, B_p, and secondary nucleation, B_s, respectively.

It is usually difficult to determine the rates of primary nucleation. Since boric acid crystallization takes place after complete dissolution of oxalic acid crystals and the solution remains clear for at least 30 seconds (see Figures 1 and 2 for run R7), it is here assumed the nucleation starts only after complete dissolution of reactant seeds. If we assume that the primary nucleation rate is dominant at least until the appearance of the first fine crystals, it is possible to estimate the rates of primary nucleation by:

$$B_p = \frac{m_{o,\,t=t_a}}{t_a - t_d} \tag{11}$$

where B_p = primary nucleation rate, number (kg free water)$^{-1}$s^{-1}; $m_{o,\,t=t_a}$ = total number of product crystals at time of t_a, number (kg free water)$^{-1}$; t_a = time of appearance of first fine crystals of boric acid; t_d = time of complete dissolution of oxalic acid crystals.

This approach assumes primary nucleation is dominant for $t_d < t < t_a$, since the magma density, and thus the secondary nucleation rate is very small during this period. The value of $m_{o,\,t=t_a}$ can be determined from the zeroth moment of the CSD obtained from the Coulter counter.

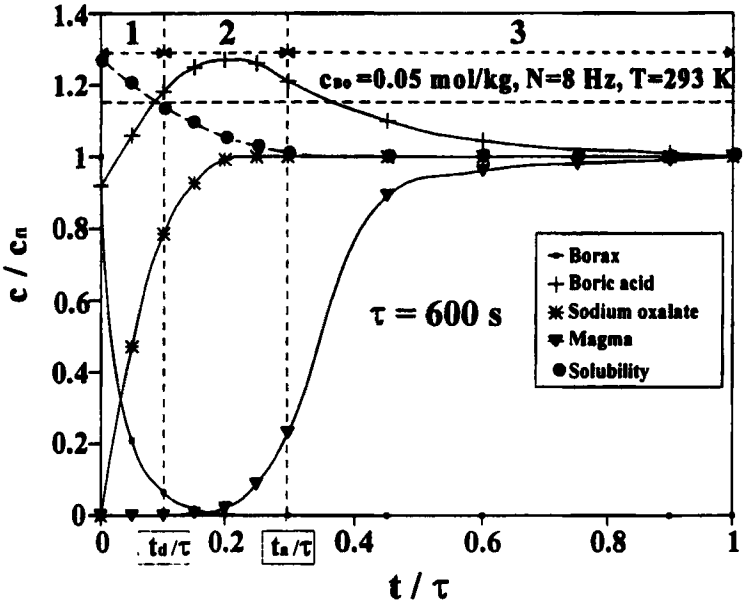

Figure 1. *Normalized species concentration and solubility profiles in run R7.*

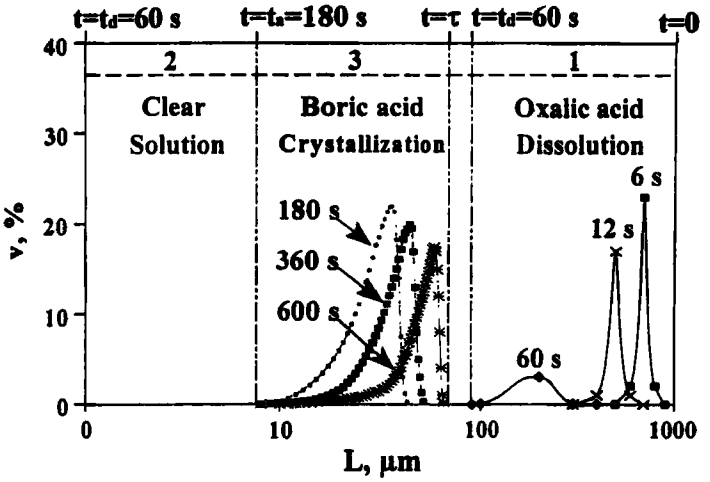

Figure 2. *Differential volume percentage of the reactant and product crystals in R7.*

The slope and the intercept of the plot of ln B_p versus T^{-3} (ln S)$^{-2}$ (see first term of Equation 10) were determined by least squares regression analysis of experimental data obtained from different runs. It was found that the results for different temperatures lie on different straight lines. The first term of Equation (10) shows that at a given supersaturation ratio, the only physical quantity which could vary with temperature is the surface energy, γ. From the slope of the straight lines obtained, the surface energy of boric acid crystals at different temperatures were evaluated, and correlated as:

$$\gamma = \gamma_0 \exp(E_\gamma/RT) \tag{12}$$

The surface energy constant, γ_o, and surface activation energy, E_γ, at 95% confidence limits were $(3.73 \pm 0.6) \times 10^{-3}$ mJ m^{-2} and 19.49 ± 2.3 kJ mol^{-1} respectively.

The apparent surface energy decreases with an increase in temperature, ranging from 11.2 mJ m^{-2} at 293 K to 7.4 mJ m^{-2} at 309 K. The primary nucleation rate coefficient, K_p, was estimated to be approximately 7.94×10^8 number kg^{-1} s^{-1}. The evaluated surface energies are significantly smaller than the true surface energy of boric acid, which is quoted as approx. 52.7 mJ m^{-2} (Mullin, 1993). This suggests the occurrence of heterogeneous primary nucleation at the supersaturation levels investigated in this work.

The secondary nucleation rates in Equation (10) can be estimated by subtracting the primary nucleation rates at a given supersaturation ratio from the measured overall nucleation rates. The method of s-plane analysis was used to determine the overall nucleation rates (Tavare and Garside, 1986). Using the calculated apparent surface energy of boric acid, the calculated values of the secondary nucleation rates of all runs have been correlated in terms of the significant process variables. The exponent in the second term in Equation (10) was estimated by least square multiple linear regression analysis and the results are tabulated in Table 2. The coefficient of determination, R^2-value, showed that a good correlation was obtained.

Table 2. *Calculated constants for the secondary nucleation rate.*

Constants and exponents for B_S in Equation (10)				
K_s, number kg^{-1} s^{-1}	***b***	***J***	***h***	***E_s, kJ mol^{-1}***
$(5.84 \pm 0.21) \times 10^8$	2.10 ± 0.22	1.31 ± 0.06	1.86 ± 0.12	12.62 ± 3.72
R^2-value = 0.883				

The exponent on magma density, 1.31, adds weight to the suggestion that secondary nucleation is important. The exponent on stirrer speed, 1.86, also shows an increase in secondary nucleation rate as the impeller speed is increased. Using the obtained exponents, the overall nucleation rates can be predicted by Equation (10). The predicted and measured overall nucleation rates for all runs are compared in Figure 3. Considering the assumptions made in the calculations, Equation (10) represents a good prediction of the overall nucleation rates.

Growth kinetics

Correlating the measured overall growth rates by s-plane method (Tavare and Garside, 1986) in terms of a power law function showed that the growth rates were proportional to $(S-1)^{1.53}$ $N^{0.75}$. Thus both surface integration and diffusion are important in the growth process. These two steps can be represented by the equations:

$$G = \phi k_d (c_{BA} - c_{BAi}) \qquad \text{Bulk diffusion} \tag{13}$$

$$G = k_r (c_{BAi} - c_{BA}^{*})^r \qquad \text{Surface integration} \tag{14}$$

where $\phi = k_F \rho_l / 3\rho_s = k_A \rho_l / 3k_v\rho_s$ and k_A and k_v are the surface and volume shape factors. Assuming that the boric acid crystals are spherical, $k_F = 6$; c_{BA} and c_{BAi} are the bulk and interfacial concentrations. The interfacial concentration, c_{BAi} in Equations (13) and (14) may be eliminated to give:

$$\frac{G}{k_d \phi} + \left(\frac{G}{k_r}\right)^{1/r} = \Delta c \tag{15}$$

Using Arrhenius-type expressions for the temperature dependency of k_d and k_r, and neglecting the first term of Equation (4) at the turbulent condition, then Equation (15) can be written as:

$$\frac{G}{k_{do}\phi N^{0.58} L^{-0.22} \exp(-E_d/RT)} + \left(\frac{G}{k_{ro}\exp(-E_r/RT)}\right)^{1/r} = \Delta c \tag{16}$$

In Equation (16), G, L, and Δc can be measured from the experiments, leaving five parameters k_{do}, k_{ro}, E_d, E_r and r to be determined. A random search method was used for parameter estimation (Edgar and Himmelblau, 1988). The objective function ε to be minimized is a relative mean square error defined as:

$$\varepsilon = \sqrt{\sum_{i=1}^{n} \frac{\left[\left(\frac{\Delta c_{i,exp}}{\Delta c_{i,calc}}\right) - 1\right]^2}{n}} \tag{17}$$

Thus the optimization is defined by minimizing the sum of squares of the supersaturation residuals. In order to find the converged solution of the problem, initial estimates of E_d, E_r and r were used. Using bulk-phase data for pure water, the activation energy for volume diffusion was estimated as $E_d = 9$ kJ/mol. Also accepting

the dependence of k_r on diffusion coefficient and solubility (Mersmann, 1992), the activation energy for surface integration was estimated as E_r = 40 kJ/mol and using the diffusion coefficient of boric acid in water of $D_{BA} = 8.8 \times 10^{-10}$ m^2s^{-1} and solubility of c^*_{BA} = 0.05 kg/kg at 293 K (Broul et al., 1981). According to the surface diffusion model (Garside et al., 1979) the value of r is between 1 and 2. Thus the initial value of this parameter was estimated as r = 1.5. Using these initial estimates, the final results of the five parameter optimization of Equation (16) are shown in Table 3. Values of the model parameters were determined by regression analysis of 100 data points from 24 experimental runs. The standard error in parameter estimates was determined at 95% confidence limits.

Table 3. *Values of the parameters for Equation (16).*

Optimization Results				
$k_{do} \times 10^3$, $m\,s^{-1}$	$k_{ro} \times 10^{-5}$, $m\,s^{-1}$	E_d, $kJ\,mol^{-1}$	E_r, $kJ\,mol^{-1}$	r
4.79 ± 0.27	2.52 ± 0.22	15.6 ± 0.08	44.2 ± 1.82	2.07 ± 0.1
ε 4.3×10^{-3}				

The order of surface integration with respect to supersaturation is found to be approximately 2. Assuming this value, then in order to examine the accuracy of the proposed kinetics, Equation (15) can be written in explicit form as:

$$G = \phi k_d \Delta c + \frac{(\phi k_d)^2}{2k_r}[1 - [1 + \frac{4k_r \Delta c}{\phi k_d}]^{1/2}] \tag{18}$$

Also using the values of parameters from Table 3, the Arrhenius-type correlations for k_d and k_r can be derived, given by Equations (19) and (20) as follows:

$$k_d = 4.79 \times 10^{-3} \exp(-1876.3/T)\, L^{-0.22}\, N^{0.58} \tag{19}$$

$$k_r = 2.52 \times 10^5 \exp(-5316.3/T) \tag{20}$$

The relationship between the measured and predicted growth rates (see Equation 18) for all runs are shown in Figure 4. The predicted growth rates are in good agreement with the measured values.

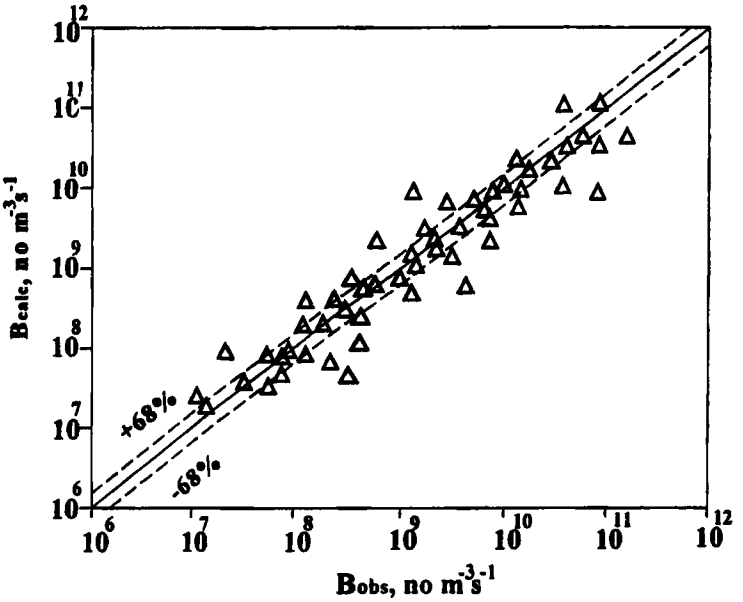

Figure 3. Comparison between the observed and calculated nucleation rates.

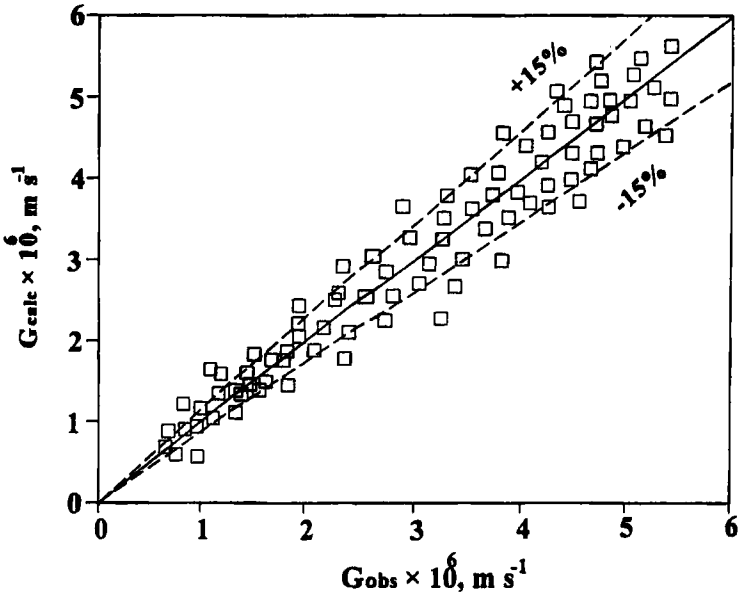

Figure 4. Comparison between the observed and calculated growth rates.

To examine the relative influence of volume diffusion and surface integration, the effectiveness factor (Garside, 1971) is calculated for a typical run (R24) with parameters obtained from Table 3:

$$\eta = \frac{G}{k_r (\Delta c)^r} \tag{21}$$

At low supersaturation ratio of approx. 1.2, the effectiveness factor is about 0.63 implying that both steps are important. At higher supersaturation ratio of approx. 2.2, the value of η declines to about 0.14 showing that here bulk diffusion resistance dominates.

(iii) Population balance and supersaturation ratio

For a perfectly mixed batch crystallizer in which crystal breakage and agglomeration are negligible, the equations obtained by moment transformation of the population balance equations (Randolph and Larson, 1988) for size independent growth rate are:

$$\frac{dm_o}{dt} = B \tag{22}$$

$$\frac{dm_i}{dt} = i\, m_{i-1} G \tag{23-25}$$

where i = 1, 2, 3 (Equations 23, 24, 25 respectively); $m_o(0)$ and $m_i(0)$ are zero for unseeded operation.

The dependence of boric acid supersaturation ratio on temperature, borax and sodium oxalate concentrations is well correlated by the following equation (ZareNezhad and Garside, 2003):

$$S = c_{BA} / [4.066\times10^{-8} T^{3.38} \exp(-15177\, T^{-1} - 12.10 c_{S.ox} + 30.05 c_B^{1.57})] \tag{26}$$

The experimental results indicate that at a fixed temperature and sodium oxalate concentration the boric acid supersaturation ratio decreases as the borax concentration is increased. Also at a given operational condition, the boric acid supersaturation ratio increases as the sodium oxalate concentration in the solution phase increases. Equation (26) is used to determine the supersaturation ratio of boric acid in the solution phase resulting from the reaction of borax solution with oxalic acid crystals.

Results and Discussions

Process simulation analysis was carried out using Equations (2) to (26). Initially only dissolution takes place until the concentration of the boric acid, c_{BA}, reaches the saturation point (S = 1). As soon as the solution becomes supersaturated with respect to boric acid, nucleation and subsequent evolution of crystal size distribution via growth commences. Consequently only the equations describing the solid reactant conversion and product concentration profiles (Equation 4 and Equations 7 to 9) are integrated initially (the second term in Equation (8) is set to zero) until the supersaturation ratio becomes unity. Once the reaction mixture becomes supersaturated with respect to boric acid the set of equations (Equations 4, 7 to 9, and 22 to 26) along with the nucleation and growth kinetics expressions (Equations 10 and 18) are solved simultaneously.

All the differential equations involved were integrated by the fourth-order Runge-Kutta method. The integration step length was set to 0.1 seconds until the supersaturation ratio became unity. As soon as supersaturation was generated the integration step length was set to 0.5 seconds. The calculations were continued until the specified end time of the process was reached.

The measured and simulated supersaturation profiles at a stirrer speed of 8 Hz and for different initial concentrations are compared in Figure 5. The simulation results show a significant increase in the peak supersaturation ratio and a faster decrease in supersaturation levels as the initial concentration is increased. There is an increase in the rate of supersaturation generation during the dissolution process as the initial reactant concentrations are increased. The initial rapid decrease in the measured supersaturation ratio corresponds to the high values of growth rate determined in the initial periods of desupersaturation. The simulation results reproduce the dissolution profiles and the S-shaped curves of the observed desupersaturation profiles, and are in relatively good agreement with experimental measurements.

Figure 6 shows the comparison between the simulated and measured variations of the number concentration of the crystals at initial concentration (c_{B0}) of 0.1 molal and different stirrer speeds. Simulation results agree well with experimental measurements in the initial periods of desupersaturation, where the influence of impeller speed is negligible, because heterogeneous primary nucleation (see section ii) was the dominant nucleation mechanism. The simulation results also show the influence of stirrer speed on secondary nucleation in the later periods of solution desupersaturation.

Simulated and measured normalized magma densities at an initial concentration (c_{B0}) of 0.07 mol/kg and different stirrer speeds are compared in Figure 7, where M_T is the magma density; M_{TT} is the total initial magma (for dissolution process) or the total final magma density (for precipitation process); τ is the time of completion of the precipitation process. The simulation results in Figure 7 show a faster decrease in the concentration of the reactant crystals (oxalic acid) during the dissolution process, and a faster increase in the magma density of the product (boric acid) during the crystallization process, as the stirrer speed is increased. The deviations between predicted and measured magma densities in the later stages of the precipitation process are larger especially at higher stirrer speeds.

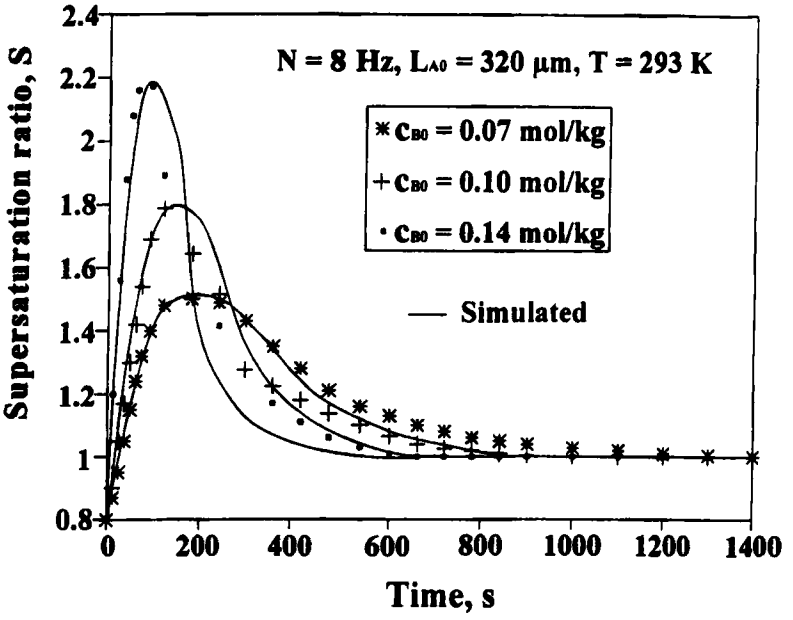

Figure 5. *Comparison of the simulated and measured supersaturation profiles at N = 8 Hz and different initial reactant concentrations.*

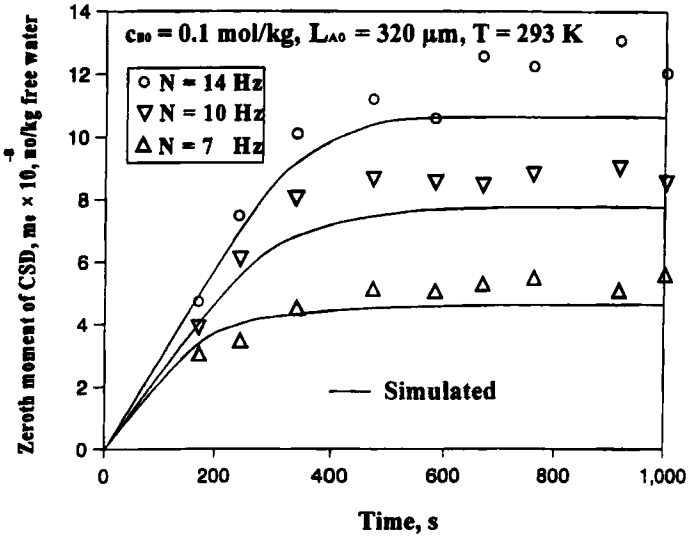

Figure 6. *Comparison of the simulated and measured number of product crystals for different stirrer speeds.*

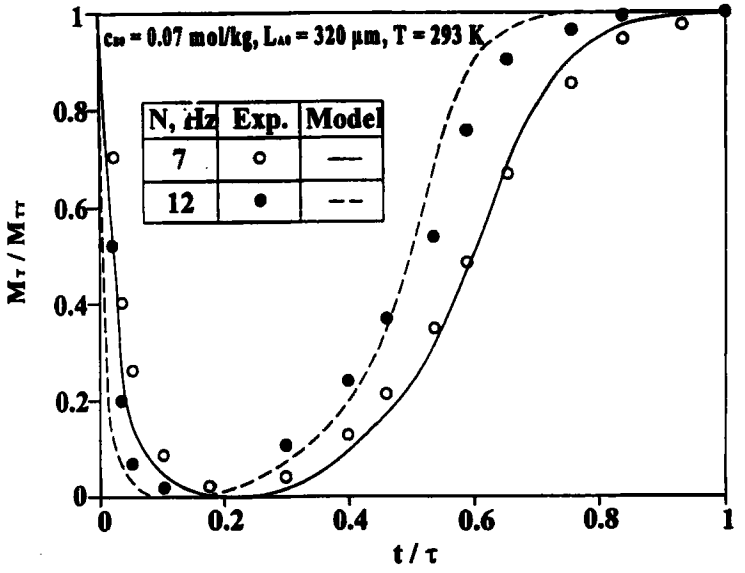

Figure 7. Comparison of the simulated and measured normalized magma density for different stirrer speeds.

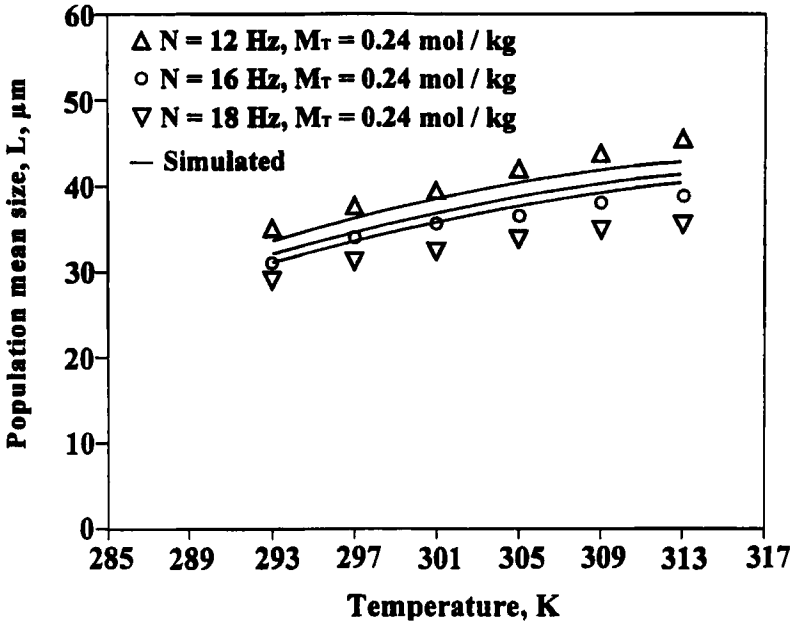

Figure 8. Comparison of the simulated and measured population mean size.

The simulations results in Figures 5 to 7 agree with experimental results better at lower stirrer speeds and initial concentrations, than at higher stirrer speeds and initial concentrations. The discrepancies observed may be due to the difficulties that were found in expressing the term for secondary nucleation by the power law equation (see section ii).

Figure 8 shows the comparison between the measured and simulated mean crystal size at different temperatures and stirrer speeds. The simulation results indicate that an increase in temperature leads to an increase in population mean size of the boric acid crystals. According to experimental observations, the influence of stirrer speed on mean crystal size is more significant at higher temperatures. This can be explained by the fact that larger crystals produced at higher temperatures are more susceptible to secondary nucleation. The simulations indicate that the population mean size decreases slightly with increased stirrer speed, while the population average size increases as initial concentration decreases. Overall, the simulation results give relatively good representation of the experimental data as shown in Figure 5 to 8.

Conclusions

Reactive dissolution of oxalic acid crystals in borax solution followed by precipitation of the product boric acid was investigated. Results obtained from analyses of the solution and solid phases were used for determination of the oxalic acid dissolution and boric acid precipitation kinetics. A diffusion-controlled surface reaction model considering particle shrinkage was used for modelling the dissolution process. Using the measured crystal size distributions, the nucleation and growth rates of boric acid crystals were evaluated by the method of S-plane analysis. Nucleation rates were influenced by heterogeneous primary nucleation and secondary nucleation, while the growth rates of product crystals were affected by both the bulk diffusion and surface integration processes.

Modelling of the product nucleation and growth kinetics are presented. The process simulation agrees with the experimentally observed supersaturation profiles at different operating conditions. The rate of supersaturation generation during the dissolution of oxalic acid crystals increases more rapidly as the impeller speed and initial concentration increases, while the supersaturation level decreases more rapidly during the crystallization process as the stirrer speed and initial concentration increases. The simulated and observed variations of the zeroth moment of crystal size distribution are in relatively good agreement. It is demonstrated that the final number concentration of the crystals increased with increasing initial concentration and stirrer speed. From the simulation results, the population mean size of boric acid crystals decreases as the stirrer speed is increased, while an increase in temperature results in an increase in the mean size of the product crystals. Simulated magma densities and crystal mean population sizes are also in good agreement with measured values.

Nomenclature

A_{ex}	External surface of oxalic acid crystals, m^2
B_p	Primary nucleation rate, number (kg free water)$^{-1}$ s^{-1}
B_s	Secondary nucleation rate, number (kg free water)$^{-1}$ s^{-1}
c_B	Concentration of borax in the solution, mol (kg free water)$^{-1}$
c_{BA}	Concentration of boric acid in the solution, mol (kg free water)$^{-1}$
c^*_{BA}	Saturation concentration of boric acid in the solution, mol (kg free water)$^{-1}$
c_{BAi}	Concentration of boric acid in the liquid film, mol (kg free water)$^{-1}$
$c_{S.ox}$	Concentration of sodium oxalate in the solution, mol (kg free water)$^{-1}$
c_{fi}	Initial or final concentration of a species, mol (kg free water)$^{-1}$ (in Figure 1)
c	Concentration of a species, mol (kg free water)$^{-1}$ (in Figure 1)
Δc	Supersaturation, mol (kg free water)$^{-1}$
D_A	Diffusion coefficient of borax in the bulk solution, m^2s^{-1}
D_{BA}	Diffusion coefficient of boric acid in the pure water, m^2s^{-1}
D	Impeller diameter, m
E_s	Activation energy for secondary nucleation, kJ (mol)$^{-1}$
E_d	Activation energy for volume diffusion, kJ (mol)$^{-1}$
E_r	Activation energy for surface integration, kJ (mol)$^{-1}$
E_γ	Activation energy of the surface, kJ (mol)$^{-1}$
G	Growth rate, ms^{-1}
K	Boltzmann constant (=1.38 × 10^{-23}), J K^{-1}
K_p	Primary nucleation rate coefficient, no (kg free water)$^{-1}$ s^{-1}
K_s	Secondary nucleation rate coefficient, no (kg free water)$^{-1}$ s^{-1}
k_d	Solid-liquid mass transfer coefficient, ms^{-1}
k_r	Surface integration rate constant, ms^{-1}
k_{do}	Bulk diffusion constant used in Equation (16), ms^{-1}
k_{ro}	Surface integration constant used in Equation (16), ms^{-1}
k_v	Volume shape factor
k_A	Surface shape factor
k_F	(= k_A / k_v)
L_A	Mean size of oxalic acid crystals, m
L	Mean size of boric acid crystals, m
M	Mass of free water, kg
M_T	Magma density, kg (kg free water)$^{-1}$
m_o	Zeroth moment of CSD, no (kg free water)$^{-1}$
m_i	i^{th} moment of CSD, number-m^i (kg free water)$^{-1}$ for i = 1, 2, 3
N	Stirrer speed, Hz
N_s	Number of moles of oxalic acid crystals, mol
N_{so}	Initial number of moles of oxalic acid crystals, mol
n	Number of experiments
R	Gas constant (= 8.314), J mol^{-1} K^{-1}
R_A	Rate of disappearance of solid oxalic acid, mol $m^{-2}s^{-1}$
R^2	Coefficient of determination (between 0 and 1)
r	Order of surface integration rate
S	Supersaturation ratio (= c_{BA} / c^*_{BA})

T Temperature, K
t Time, s
V Solution volume, m^3
v Differential volume percentage of crystals (in Figure 2)
X Fractional conversion of oxalic acid crystals

Greek symbols

ε Relative mean square error (Equation 17)
η Effectiveness factor
ρ_l Density of free water, kg m^{-3}
ρ_s Molar volume of solid phase, mol m^{-3}
γ Surface energy, (mJ) m^{-2}
γ_o Surface energy constant, (mJ) m^{-2}
α Sphericity (= 16π /3)
ν Kinematic viscosity, m^2s^{-1}
β Stoichiometric ratio of the reactants(= 1)
ϕ Overall shape factor, (kg free water) mol^{-1}
φ Molecular volume, m^3 kg^{-1}
τ Time of completion of the process, s

References

Asai, S., Konishi, Y., and Sasaki, Y. 1986. Mass transfer between fine particles and liquids in an agitated vessel. *Third World Congress of Chem. Eng.*, Tokyo, Japan, Part **II**, 428-430.

Broul, M., Nyvlt, J., and Shnel, O. 1981. Solubility in Inorganic Two-Component Systems, Elsevier Scientific Publishing Co., Amsterdam.

David, R., and Bossoutrot, J.M. 1996. The modelling of sodium perborate tetrahydrate crystallization from solution. *Chem. Eng. Sci.*, **51**(21), 4939-4947.

Edgar, T.F., and Himmelblau, D.M. 1988. Optimization of Chemical Processes, McGraw-Hill, USA.

Franck, R., David, R., Villermaux, J.A., and Klein, J.P. 1988. Crystallization and precipitation engineering. *Chem. Eng. Sci.*, **43**, 69-77.

Garside, J. 1971. The concept of effectiveness factors in crystal growth. *Chem. Eng. Sci.*, **26**, 1425-1431.

Garside, J., Rusli, I.T., and Larson, M.A. 1979. Origin and size distribution of secondary nuclei. *AIChE J.*, **25**, 57-64.

Jeffery, G.H., Bassett, J., Mendham, J., and Denney, R.C. 1989. Vogel's Textbook of Quantitative Chemical Analysis, Fifth Edition, Longman Group, UK.

Mersmann, A., Angerhfer, M., Gutwald, T., and Wang, S. 1992. General prediction of median crystal sizes. *Sep. Technol.*, **2**, 85-90.

Mullin, J.W., 1993, Crystallization, Butterworth-Heinemann, London.

Randolph, A., and Larson, M. 1988. Theory of Particulate Processes, Academic Press, San Diego, USA.

Tavare, N.S., and Garside J. 1990. Simulation of reactive precipitation in a semi-batch crystallization. *Chem. Eng. Res. Des.*, **68**, 115-122.

Tavare, N.S., and Garside J. 1986. Simultaneous estimation of crystal nucleation and growth kinetics from batch experiments. *Chem. Eng. Res. Des.*, **64**, 109-118.

Wachi, S. and Jones, A.G., 1991. Mass transfer with chemical reaction and precipitation. *Chem. Eng. Sci.*, **46**, 1027-1033.

ZareNezhad, B., Manteghian, M., and Tavare, N.S. 1996. On the confluence of dissolution, reaction and precipitation. *Chem. Eng. Sci.*, **51**(11), 2547-2552.

ZareNezhad, B., 1996. Crystal size distribution control in reactive precipitation processes. *Dev. Chem. Eng. Mineral Process.*, **4**(3), 213-222.

ZareNezhad, B. and Garside, J. 2003. Solubility of boric acid in the mixtures of borax and sodium oxalate, accepted for publication in *J. Chem. & Eng. Data.*

Received: 24 April 2002; *Accepted after revision:* 3 March 2003.